2010 IEEE International Conference on Robotics and Automation
Anchorage Convention District
May 3-8, 2010, Anchorage, Alaska, USA

Walking speed estimation using shank-mounted accelerometers

E. Bishop and Q. Li

Abstract— **We studied the feasibility of estimating walking speed using two shank-mounted accelerometers. Our approach took advantage of the inverted pendulum-like behavior of the stance leg during walking to identify a new method for dividing up walking into individual stride cycles and estimating the initial conditions for the direct integration of the accelerometer signals. To test its accuracy, we compared speed to known values during treadmill walking. The speed estimation method worked well across treadmill speeds yielding a root mean square speed estimation error of only 8%. This accuracy is comparable to that achieved from shank-mounted inertial measurement unit, providing a robust and low-cost alternative in using accelerometer for walking speed estimation. Shank-mounted accelerometer may be of great benefit for estimating speed in walking for the embedded control of knee-mounted devices such as prostheses and energy harvesters.**

I. INTRODUCTION

An important component of gait analysis is the determination of walking's spatial and temporal parameters including heel strike, toe-off, cadence, stride length and walking speed. These parameters are useful for diagnosing abnormal gait, evaluating the effectiveness of rehabilitation techniques, control of energy harvester and exoskeleton [1], [2], [3], [4], [5], [6]. Optical motion analysis systems along with force platforms provide a complete gait analysis system; however they are expensive, sophisticated, require a dedicated laboratory, and the set up and data analysis is timely. Recent efforts have focused on portable gait analysis systems using accelerometers and gyroscopes. Accelerometers measure acceleration, gyroscopes measure angular velocity, and inertial measurement units (IMUs) are the combination of both sensors. Most studies using accelerometers and gyroscopes have been concerned with estimating temporal gait parameters—such as stride frequency—from characteristic features in the sensor signals when attached to different body locations including the truck, thigh, shank and foot [7], [8], [9], [10].

Determining walking speed requires estimating stride length in addition to stride frequency. One approach estimates stride length indirectly by first computing segment angles from gyroscope measurements and then relating the stride length to the computed angles using an anthropomorphic model. Miyazaki integrated angular velocity measured by a thigh-mounted gyroscope to determine thigh angle [11]. A single element model related thigh angle to stride length resulting in an error in estimated speed of less than 15%. Aminian *et. al.* used a more realistic two-segment model with gyroscopes mounted on the thigh and shank and achieved a root mean square estimation error of 7% [12]. While these studies demonstrate reasonable accuracy in estimating speed, they are limited by their requirement of subject-specific calibration—the same angles in a taller person will correspond to longer stride lengths and faster speeds. Instead of estimating spatial parameters indirectly, an alternative is to determine displacements by direct time integration of measured accelerations. This approach is more general than the previously described indirect approach as it does not require subject-specific calibration. It requires the acceleration measurements and continuous knowledge of the device angle with respect to gravity to subtract gravitational acceleration. Consequently, IMU has been attached at lower-limb locations to estimate walking speeds. A foot mounted IMU was used by [13] to estimate spatio-temporal gait parameters. Gait phase segmentation and strapdown integration resulted in root mean square speed estimation errors of about 5%. Li *et. al* used a shank mounted IMU to estimate walking speed and achieved comparable results with a root mean square speed estimation error of 7% [14].

Accelerometers are significantly lower in power consumption and cost than gyroscopes, and demonstrate a high degree of reliability in measurement with little variation over time [15]. Due to recent breakthrough developments in micro-machining technology, the costs of micro-machined accelerometers are decreasing while the accuracy is being improved. Accelerometers have less fundamental physical constraints than gyroscopes, so the precision of a micro-machined accelerometer is less inhibited than the precision of a micro-machined gyroscope. Zijlstra and Hof studied the feasibility of estimating spatio-temporal gait parameters using a trunk-mounted accelerometer. From the measured upward and downward displacements of the trunk, an inverted pendulum model estimated mean step length yielding root mean square speed estimation errors ranging from 5% at a walking speed of 0.5 m/s to 14% at a walking speed of 1.75 m/s [16]. While this approach is quite useful in estimating spatio-temporal gait parameters, it is limited by its requirement of subject-specific calibration—the same angles in a taller person will correspond to longer stride lengths and faster speeds. Moreover, it is not always desirable to mount sensors directly on the trunk. During walking, the support moments generated at the ankle, knee and hip joints of the support leg influence the measured trunk accelerations, resulting in a complex acceleration pattern [16]. Consequently, it affects the accuracy of speed estimation.

This work was partially supported by Queen's ARC grant to Q. Li.

E. Bishop is with Department of Mechanical and Manufacturing Engineering, and McCaig Centre for Joint Injury and Arthritis Research, University of Calgary, Calgary, AB, Canada elbishop@ucalgary.ca

Q. Li is with the Human Mobility Research Centre, Queen's University and Kingston General Hospital, Kingston, and the Department of Mechanical and Materials Engineering, Queen's University, Kingston, Ont. K7L 3N6 Canada. qli@mech.queensu.ca

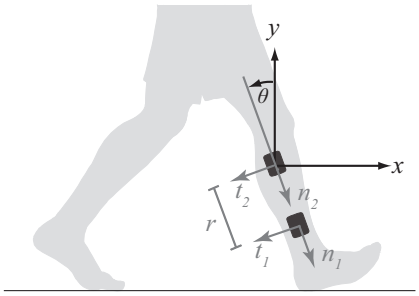

Fig. 1. Sensor configuration. Two inertial measurement units (IMUs) are attached to the shank in the sagittal plane on the lateral side. The normal accelerations a_{n1} and a_{n2} are measured along the n direction, and the tangential accelerations a_{t1} and a_{t2} are measured along the t direction. The arrows indicate positive axes for the corresponding sensor measurements. The world coordinate is defined by the x and y axes, and the vertical axis y extends in a direction parallel to gravity.

In addition, mounting sensors closer to the knee joint would be more useful for the embedded control of knee-mounted devices such as prostheses, orthoses, exoskeletons and energy harvesters [17], [18], [6], [5]. This study uses the acceleration signals from two shank-mounted inertial measurement units (IMUs) to estimate walking speed. Our approach uses the relationship between two tangential accelerations on a rigid body to obtain its position in space. To test its accuracy, we compared algorithm speed estimates to known values during treadmill walking at a range of speeds.

II. Methods

A. Speed estimation

Two wireless inertial measurement units (IMUs) were used to measure shank linear accelerations. Each IMU (MicroStrain Inertia-Link) contained an accelerometer and a gyroscope. When the shank is vertical with respect to the world coordinate system, the tangential and normal axes of the accelerometer point in the fore-aft and vertical directions, respectively (Figure 1). The shank angle, θ, is defined as the angle between the negative normal axis of the accelerometer and the vertical axis of the world coordinate system.

The tangential acceleration components from two accelerometers on a rigid body relate directly to angular acceleration. The shank angular acceleration, $\alpha(t)$, was calculated using the accelerometer-measured tangential acceleration signals $a_{t1}(t)$ and $a_{t2}(t)$,

$$\alpha(t) = \frac{a_{t2}(t) - a_{t1}(t)}{r}, \tag{1}$$

where *r* is the distance separating the sensors (Figure 1). The angular acceleration is filtered using both a high pass filter (0.3 Hz cutoff 2nd order Butterworth) and a low pass filter (2.5 Hz cutoff 2nd order Butterworth) before the computation. The shank angular velocity $\omega(t)$ was computed by integrating the angular acceleration $\alpha(t)$,

$$\omega(t) = \int_0^t \alpha(\tau)d\tau + \omega(0), \tag{2}$$

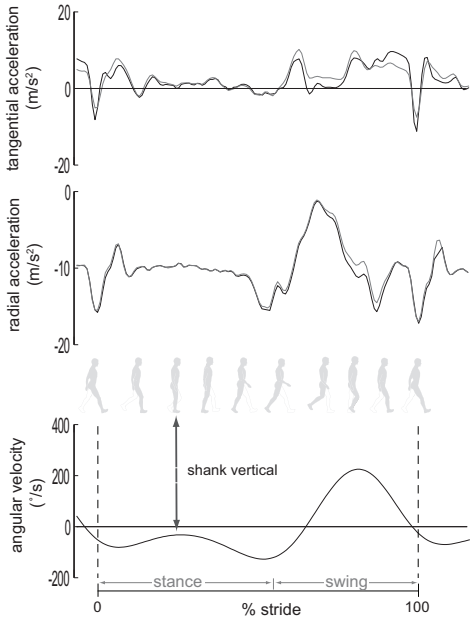

Fig. 2. Tangential acceleration a_t, radial acceleration a_n and calculated angular velocity ω. Accelerations from the low sensor are black, and from the high sensor are grey. The angular velocity is filtered.

using an initial value $\omega(0)$=0. Following integration, the angular rate is filtered using a high pass filter (0.3 Hz cutoff 2nd order Butterworth) to eliminate the constant offset that causes drift.

To compute the displacements along the horizontal and vertical world coordinate axes, we first resolved the filtered (2.5 Hz cutoff 2nd order Butterworth) acceleration signals $a_n(t)$ and $a_t(t)$ into component accelerations $a_x(t)$ and $a_y(t)$ in the world coordinate system according to

$$\begin{aligned} a_x(t) &= a_n(t)\sin\theta(t) - a_t(t)\cos\theta(t) \\ a_y(t) &= -a_n(t)\cos\theta(t) - a_t(t)\sin\theta(t) - g, \end{aligned} \tag{3}$$

where $\theta(t)$ is the shank angle, and g is the acceleration due to the gravity (Figure 1). This calculation was performed using the acceleration signals from the upper sensor, the lower sensor, and the average signal (resulting in three speed estimation methods). The shank angle $\theta(t)$ was computed by integrating the angular velocity $\omega(t)$,

$$\theta(t) = \int_0^t \omega(\tau)d\tau + \theta(0), \tag{4}$$

where $\theta(0)$ is the initial shank angle before integration. With the resolved accelerations $a_x(t)$ and $a_y(t)$, we computed the associated velocities $v_x(t)$ and $v_y(t)$,

$$\begin{aligned} v_x(t) &= \textstyle\int_0^t a_x(\tau)d\tau + v_x(0) \\ v_y(t) &= \textstyle\int_0^t a_y(\tau)d\tau + v_y(0), \end{aligned} \tag{5}$$

where $v_x(0)$ and $v_y(0)$ are the initial horizontal and vertical velocity conditions.

By integrating the velocities $v_x(t)$ and $v_y(t)$, we obtained the horizontal displacement, $s_x(t)$, and vertical displacement,

$s_y(t)$,

$$\begin{aligned} s_x(t) &= \int_0^t v_x(\tau)d\tau + s_x(0) \\ s_y(t) &= \int_0^t v_y(\tau)d\tau + s_y(0), \end{aligned} \tag{6}$$

where $s_x(0)$ and $s_y(0)$ are the initial horizontal and vertical positions before the start of integration.

The continuous walking motion was segmented into a series of stride cycles, resetting the integration of Equations (4)-(6) at the beginning of each new cycle. Similar to the method of [14], each new stride cycle was defined by the time in the stance phase when the shank is parallel to the direction of gravity. This occurs at the local maximum during the lengthy period of negative angular velocity, as shown in (Figure 2). At this event, the initial conditions for integration were assumed to be $\theta(0) = 0$, $v_y(0) = 0$, $v_x(0) = 0$, $s_y(0) = 0$, and $s_x(0) = 0$. This allowed for the integration of Equations (4)-(6), providing a first estimate of horizontal and vertical displacements.

To reduce the estimation error caused by offsets in the acceleration measurements, we assumed zero net acceleration within each stride cycle. So, during steady state walking the shank horizontal and vertical velocities are the same at the beginning and end of the stride cycle. The horizontal velocity at the beginning of the stride, $v_x(0)$, equals zero, however offsets in the acceleration measurements result in the horizontal velocity at the end of the stride, $v_x(T)$, being nonzero. We estimated this mean horizontal acceleration offset, $\bar{a}_x$, as

$$\bar{a}_x = (v_x(T) - v_x(0))/T. \tag{7}$$

The contribution of this offset $\bar{a}_x$ to the estimated horizontal displacement was

$$\bar{s}_x = \frac{1}{2}\bar{a}_x T^2 = \frac{1}{2}T \cdot v_x(T). \tag{8}$$

Similarly, we estimated the mean vertical acceleration offset, $\bar{a}_y$, as

$$\bar{a}_y = (v_y(T) - v_y(0))/T. \tag{9}$$

The contribution of this offset to the estimated vertical displacement was

$$\bar{s}_y = \frac{1}{2}\bar{a}_y T^2 = \frac{1}{2}T \cdot v_y(T). \tag{10}$$

At the end of each gait cycle, we performed a correction on the estimated horizontal and vertical displacement of Equation (6) by subtracting the corresponding offsets from Equations (8) and (10). The corrected horizontal displacement $s'_x(T)$ and vertical displacement $s'_y(T)$ in the gait cycle were calculated as

$$\begin{aligned} s'_x &= s_x(T) - \tfrac{1}{2}T \cdot v_x(T) \\ s'_y &= s_y(T) - \tfrac{1}{2}T \cdot v_y(T), \end{aligned} \tag{11}$$

and the stride length s_T was computed as

$$s_T = \sqrt{(s'_x)^2 + (s'_y)^2}. \tag{12}$$

With the stride length s_T, we computed the average walking speed $V(T)$, in m/s, for each gait cycle as

$$V(T) = s_T/T. \tag{13}$$

Before each walking experiment, the normal axes of the accelerometers were aligned with gravity using the Inertia-Link software. During the experiment, data was collected simultaneously from both sensors at a sample rate of 100 Hz using Labview (National Instrument, TX). The speed estimation algorithm was programmed in Matlab (Mathworks, Natick, MA).

B. Experimental methods

Treadmill walking experiments were performed to test the accelerometer based walking speed estimation. Ten male and eight female subjects (age: 22.7 $\pm$ 4.7 years; height: 1.76 $\pm$ 0.09; tibia length: 0.42 $\pm$ 0.03 m) participated in the experiment. All subjects were healthy and did not exhibit any clinical gait abnormalities. The Queen's General Research Ethics Board has approved the study and subjects gave their informed consent before participating.

The volunteers performed walking at treadmill speeds of 0.8, 1.0, 1.2, 1.4, 1.6 and 1.8 m/s. Subjects walked at each of these speeds with sensor separation distances of 6.3 and 10.0 cm. The subjects wore their own athletic clothing and walking shoes during the experiments. Trials were 90s in duration. During all trials, the IMUs were mounted on a rigid plastic ruler and attached directly onto the calf parallel to the sagittal plane. The pair of sensors was secured onto the subject's skin using double sided tape and athletic tape. The midpoint between the two sensors was positioned midway between the knee and ankle along the longitudinal axis. It was expected that the sensors would not interfere with the subjects' normal walking pattern, and that vibration of the attachment would be minimal.

C. Data analysis

For each treadmill walking trial we calculated the mean walking speed by averaging the stride-by-stride data, and then calculating a moving window average (size=20) on the first $30s$ of data. Estimation error at a given speed was calculated as the difference between the estimated speed and the actual treadmill speed. Within a condition, we averaged across subjects to determine the mean estimation error (Mean) and standard derivation (S.D.). We also calculated the root mean square error (RMSE) of the speed estimates as RMSE $= \sqrt{\sum (\text{estimated-actual})^2/N}$ (N is the number of samples). For each combination of sensor separation distance and speed estimation method we calculated the RMSE between eighteen subjects across six speeds ($N = 108$). The effects of walking speed, sensor separation and estimation method on speed estimation error were tested using repeated-measures ANOVA, with $P < 0.05$ considered statistically significant.

Linear regression was performed on the mean speed estimations from eighteen subjects for all combinations of sensor separation distance and speed estimation method.

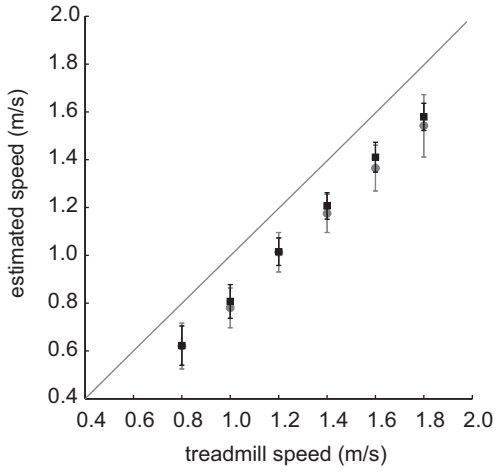

Fig. 3. Estimated speeds from lower sensor with separation distances of 10.0 cm (•) and 6.3 cm (■). The solid grey line is the line of identity where the estimated speed equals the treadmill speed. Values shown are means± S.D., $N = 18$.

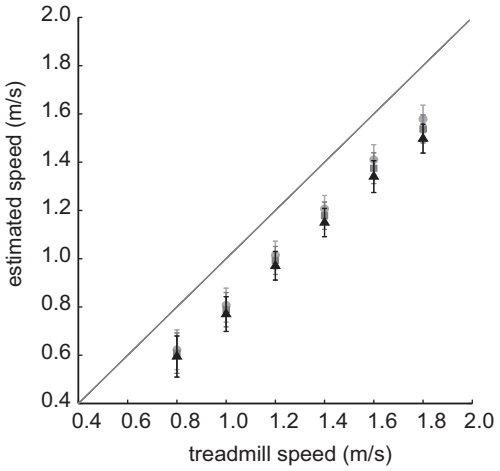

Fig. 4. Estimated speeds with separation distance of 6.3 cm using the low (•), average (■) and high (▲) sensor estimations. The solid grey line is the line of identity where the estimated speed equals the treadmill speed. Values shown are means± S.D., $N = 18$.

The y-intercept value was used to adjust the mean speed estimations such that a linear regression on the adjusted values would produce a y-intercept of zero. Estimation error and RMSE calculations were performed on the adjusted speed estimations as described above.

III. Results

The proposed speed estimation method underestimated walking speed, however the estimation errors were consistent across experimental conditions (Table 1). Figure 3 compares sensor separation distance, and while this did not affect the speed estimation error ($P = 0.18$), the algorithm tended to have slightly lower errors using a separation distance of 6.3 cm. Actual speed did not affect the speed estimation error ($P = 0.46$). The three speed estimation methods were found to have a significant effect on speed estimation error ($P = 0.02$). Figure 4 shows that the lower sensor estimation has smaller errors, the higher sensor estimation has larger errors, and the average signal estimation falls between the high and low speed estimations.

Figure 5 shows subject data with a linear fit having a slope of 0.97 and a y-intercept of -0.15 (r^2=0.98). The adjusted data accurately estimates speed with low variability. Figure 6 presents typical speed estimation data from a single subject. This pattern holds across the eighteen measured subjects as summarized in Table 1. The RMSE for the adjusted low sensor estimation using a separation distance of 6.3 cm was 0.08.

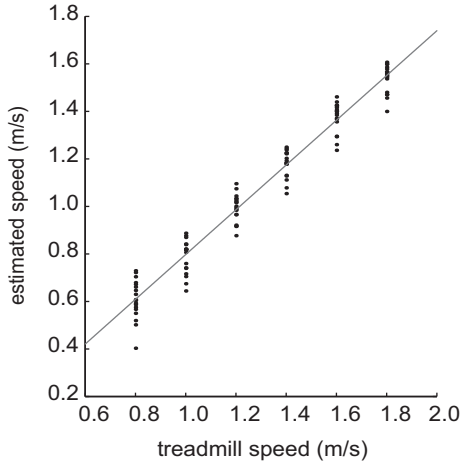

Fig. 5. Estimated speeds from the low sensor for all subjects ($N = 18$) using a sensor separation distance of 6.3 cm. The solid grey line is a linear fit to the data.

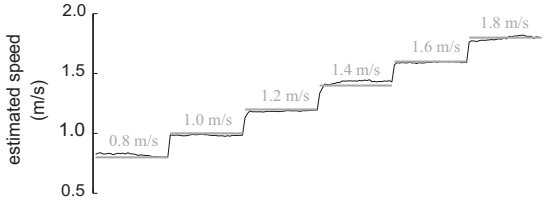

Fig. 6. Adjusted estimated speed from a representative subject using the low sensor estimation and a separation distance of 6.3 cm.

IV. Discussion

Our results indicate that two shank-mounted accelerometers can provide accurate estimates of walking speed across a wide range of speeds. This approach used the relationship between two tangential accelerations on a rigid body to obtain angular velocity. The algorithm worked well across speeds yielding a root mean square speed estimation error

TABLE I

SPEED ESTIMATION ERRORS AT DIFFERENT SPEEDS AND SEPARATION DISTANCES

Sensor Separation		Speed (m/s) 0.8	1.0	1.2	1.4	1.6	1.8	RMSE
6.3 cm	low	-0.18 ± 0.08	-0.19 ± 0.07	-0.18 ± 0.06	-0.19 ± 0.06	-0.19 ± 0.06	-0.22 ± 0.06	0.20
	low_adj	-0.03 ± 0.08	-0.04 ± 0.07	-0.03 ± 0.06	-0.04 ± 0.06	-0.04 ± 0.06	-0.07 ± 0.06	0.08
	avg	-0.19 ± 0.08	-0.21 ± 0.07	-0.21 ± 0.06	-0.22 ± 0.06	-0.22 ± 0.06	-0.26 ± 0.06	0.23
	avg_adj	-0.05 ± 0.08	-0.07 ± 0.07	-0.07 ± 0.06	-0.08 ± 0.06	-0.08 ± 0.06	-0.12 ± 0.06	0.10
	high	-0.21 ± 0.09	-0.23 ± 0.07	-0.23 ± 0.06	-0.25 ± 0.06	-0.26 ± 0.07	-0.30 ± 0.06	0.26
	high_adj	-0.07 ± 0.09	-0.09 ± 0.07	-0.09 ± 0.06	-0.11 ± 0.06	-0.12 ± 0.07	-0.16 ± 0.06	0.13
10.0 cm	low	-0.18 ± 0.10	-0.22 ± 0.08	-0.19 ± 0.08	-0.22 ± 0.08	-0.23 ± 0.10	-0.26 ± 0.13	0.24
	low_adj	-0.05 ± 0.10	-0.09 ± 0.08	-0.06 ± 0.08	-0.09 ± 0.08	-0.10 ± 0.10	-0.13 ± 0.13	0.13
	avg	-0.20 ± 0.09	-0.24 ± 0.08	-0.22 ± 0.07	-0.26 ± 0.06	-0.28 ± 0.08	-0.31 ± 0.11	0.26
	avg_adj	-0.08 ± 0.09	-0.12 ± 0.08	-0.10 ± 0.07	-0.14 ± 0.06	-0.16 ± 0.08	-0.19 ± 0.11	0.16
	high	-0.21 ± 0.08	-0.26 ± 0.07	-0.24 ± 0.06	-0.29 ± 0.06	-0.31 ± 0.07	-0.36 ± 0.09	0.29
	high_adj	-0.10 ± 0.08	-0.15 ± 0.07	-0.13 ± 0.06	-0.18 ± 0.06	-0.20 ± 0.07	-0.25 ± 0.09	0.19

low, avg, high indicate speeds estimated using low, average and high accelerometer measurements.
low_adj, avg_adj, high_adj indicate estimated speeds from linear regression.
Values are means $\pm S.D.$, $N = 18$.

of only 8% when using the adjusted low sensor estimation with a sensor separation distance of 6.3 cm.

The separation distance between the two sensors affected speed estimation results (Figure 3). The sensors were mounted on the shank, which is not a flat surface. Although a ruler was used to improve alignment, deviations from the sagittal plane affect the linear acceleration signals thereby affecting speed estimation. A smaller distance between the sensors reduces the magnitude of alignment error resulting in a decreased speed estimation error. As expected, the closer configuration (6.3 cm) provided a more accurate speed estimation than the larger separation distance (10 cm). This result is promising for the development of a portable gait speed estimation system because it allows the two accelerometers to be placed close together.

The acceleration signals (low, average and high) used in the algorithm affected speed estimation results (Figure 4). To determine the initial condition for integrating the sensor horizontal acceleration, we assumed a zero sensor horizontal velocity at mid-stance shank vertical (Equation 5). Any deviation of the actual initial horizontal velocity from zero would result in the same amount of offset in the estimated horizontal speed. Because the shank rotates about the ankle joint at the mid-stance shank vertical event, the absolute value of the initial horizontal velocity $v_x(0)$ is approximately equal to the product of the angular velocity ω of the shank and the distance of the sensor to the ankle joint. At the mid-stance shank vertical event, the shank angular velocity reached a non-zero local maximum resulting in a positive nonzero initial horizontal velocity (Figure 2). The speed estimation algorithm underestimated walking speed, and the estimation error was larger for the higher sensor because the distance from the sensor to the ankle joint was larger, resulting in a larger initial horizontal velocity at the peak of the inverted pendulum arc. This suggests that the sensors should be placed more distally on the shank for accurate speed estimation.

Although the algorithm underestimates speed, the data follows a linear trend and can be adjusted using the y-intercept value to produce very accurate speed estimations (Figure 6). This relies on a constant linear adjustment, as opposed to a multiplication factor of 1.25 used by [16]. The present accuracy is comparable to that achieved by Li et al. (2009) who used one shank mounted gyroscope, while we used two shank mounted accelerometers. The results indicated that linear correction is necessary when using accelerometers for walking speed estimation.

V. CONCLUSION

The present paper investigated the feasibility of using two shank-mounted accelerometers in walking speed estimation. By appropriately segmenting a walking sequence into gait cycles, the algorithm estimated stride-by-stride walking speed. Treadmill walking experiments demonstrated that this method could accurately estimate the walking speeds under different walking conditions.

Since spatio-temporal gait parameters have strong correlations with muscle activity and energy generation/absorption of joints during walking, real-time estimation of these parameters is critical for implementing optimal adaptive strategies for prostheses and orthoses, exoskeletons, and energy harvester control. The long term goal is to integrate gait analysis techniques with real-time signal processing methods to develop a low-cost, portable, and real-time gait parameter estimation system for wearable robotic applications.

REFERENCES

[1] TP Andriacchi, JA Ogle, and JO Galante. Walking speed as a basis for normal and abnormal gait measurements. *Journal of Biomechanics*, 10(4):261–8, 1977.

[2] JO Judge, M. Underwood, and T. Gennosa. Exercise to improve gait velocity in older persons. *Archives of physical medicine and rehabilitation*, 74(4):400–406, 1993.

[3] BE Maki. Gait changes in older adults: predictors of falls or indicators of fear. *J Am Geriatr Soc*, 45(3):313–20, 1997.

[4] CL Richards, F. Malouin, S. Wood-Dauphinee, JI Williams, JP Bouchard, and D. Brunet. Task-specific physical therapy for optimization of gait recovery in acute stroke patients. *Arch Phys Med Rehabil*, 74(6):612–20, 1993.

[5] J. M. Donelan, Q. Li, V. Naing, J. A. Hoffer, D. J. Weber, and A. D. Kuo. Biomechanical energy harvesting: generating electricity during walking with minimal user effort. *Science*, 319(5864):807–10, 2008.

[6] H. Kazerooni, R. Steger, and L. Huang. Hybrid Control of the Berkeley Lower Extremity Exoskeleton (BLEEX). *The International Journal of Robotics Research*, 25(5-6):561, 2006.

[7] R. Moe-Nilssen and J.L. Helbostad. Estimation of gait cycle characteristics by trunk accelerometry. *Journal of biomechanics*, 37(1):121–126, 2004.

[8] K. Aminian, K. Rezakhanlou, E. De Andres, C. Fritsch, P.F. Leyvraz, and P. Robert. Temporal feature estimation during walking using miniature accelerometers: an analysis of gait improvement after hip arthroplasty. *Medical and Biological Engineering and Computing*, 37(1):686–691, 1999.

[9] J. M. Jasiewicz, J. H. Allum, J. W. Middleton, A. Barriskill, P. Condie, B. Purcell, and R. C. Li. Gait event detection using linear accelerometers or angular velocity transducers in able-bodied and spinal-cord injured individuals. *Gait Posture*, 24(4):502–9, 2006.

[10] IPI Pappas, MR Popovic, T. Keller, V. Dietz, and M. Morari. A reliable gait phase detection system. *IEEE Transactions on neural systems and rehabilitation engineering*, 9(2):113–125, 2001.

[11] S. Miyazaki. Long-term unrestrained measurement of stride length and walking velocity utilizing a piezoelectric gyroscope. *Ieee Transactions on Biomedical Engineering*, 44(8):753–759, 1997.

[12] K. Aminian, B. Najafi, C. Bula, P. F. Leyvraz, and P. Robert. Spatio-temporal parameters of gait measured by an ambulatory system using miniature gyroscopes. *Journal of Biomechanics*, 35(5):689–699, 2002.

[13] A. M. Sabatini, C. Martelloni, S. Scapellato, and F. Cavallo. Assessment of walking features from foot inertial sensing. *IEEE Trans Biomed Eng*, 52(3):486–94, 2005.

[14] Q. Li, M. Young, V. Naing, and J. M. Donelan. Walking speed and slope estimation using shank-mounted inertial measurement units. In *Rehabilitation Robotics, 2009. ICORR 2009. IEEE International Conference on*, pages 839–844, June 2009.

[15] R. E. Mayagoitia, A. V. Nene, and P. H. Veltink. Accelerometer and rate gyroscope measurement of kinematics: an inexpensive alternative to optical motion analysis systems. *Journal of Biomechanics*, 35(4):537–42, 2002.

[16] W. Zijlstra and A. L. Hof. Assessment of spatio-temporal gait parameters from trunk accelerations during human walking. *Gait & Posture*, 18(2):1–10, 2003.

[17] H. Herr and A. Wilkenfeld. User-adaptive control of a magnetorheological prosthetic knee. *Industrial Robot: An International Journal*, 30(1):42–55, 2003.

[18] B. Weinberg, J. Nikitczuk, S. Patel, B. Patritti, P. Bonato, and P. Canavan. Design, Control and Human Testing of an Active Knee Rehabilitation Orthotic Device. In *2007 IEEE International Conference on Robotics and Automation*, pages 4126–4133, 2007.